Table II. Calculated Effective Masses, m^*, and Deformation Potentials, $\delta\epsilon$, for Periodic $(I_3^-)_\infty$ and $(CH)_x$ Chains

	m^*/m_{el}		$\delta\epsilon$, eV	
	electron	hole	electron	hole
$(I_3^-)_\infty$	0.10	0.09	37.4	24.7
$(CH)_x$	0.10	0.11	4.6	3.4

observed[13] within the permissible range ($\theta > 80°$) depending on the shape of the inclusion channel for the PI's. The large increase of the energy below $\theta \simeq 80°$ is due to the strong antibonding character of the orbital **4** associated with π lone pairs.

4

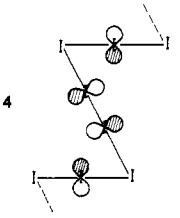

Semiconducting properties

Experimental data related to the PI chains without host are not available. In what follows we compare our theoretical results with indirect experimental information. The existence of a nonzero energy gap can be inferred for the $(I_5^-)_\infty$ systems from the optical spectrum which shows a well-known strong absorption onset around 2 eV for the starch and related nonconducting complexes[3,8b,17b] where the insulating organic host most probably has an absorption onset at higher energies. The well-conducting PI complexes do not provide direct evidences because they strongly absorb in the low-energy (IR) region because of the electronic transitions there. Our prediction of the $E_{gap} \simeq 1.8$ eV for the $(I_3^-)_\infty$ system thus cannot be confronted with experiments on these systems. Nevertheless, the theoretical trend for the gaps $I_2 > I_3^- > (I_5^-)_\infty > (I_3^-)_\infty$ should be verifiable.

The degree of electron (or hole) delocalization should be larger for $(I_3^-)_\infty$ than for $(I_5^-)_\infty$ as follows immediately from the energy band widths. The band width is in the order of 1.5 eV for $(I_3^-)_\infty$, 0.5 eV for linear $(I_5^-)_\infty$, and 0.1 eV for strongly bent $(I_5^-)_\infty$. Thus $(I_5^-)_\infty$ is coming electronically close to narrow band insulators, as typical organic molecular crystals. $(I_3^-)_\infty$ resembles in this respect the polymeric semiconductors, like undoped polyacetylene $(CH)_x$.[29] This can be also seen from the calculated effective mass values given in Table II. It would be, however, more important to compare the mobilities of the charge carriers, μ. The theoretical estimation of the latter is very difficult, owing partly to the great number of possible scattering mechanisms. One important channel, the interaction with acoustic vibrations, can be approximately characterized by the deformation potential[30] $\delta\epsilon$

$$\delta\epsilon = \Delta E/(\delta a/a)$$

where va is a uniform dilation of the lattice constant a and ΔE the corresponding shift of the edge of the energy band. These are then roughly related[30] as $\mu \simeq (\delta\epsilon)^{-2}$. This indicates that, other factors being equal, electron and hole mobilities in $(I_3^-)_\infty$ are expected to be small compared with those in $(CH)_x$. In most of the real PI complexes, disorder effects[31] may dominate the transport properties.

Acknowledgment. This work has been partly supported by the KKA Project of the Hungarian Academy of Sciences.

Registry No. I_3^-, 14900-04-0; I_5^-, 22318-17-8.

(29) (a) H. Shirakawa, T. Ito, and S. Ikeda, *Makromol. Chem.*, **179**, 1565 (1978); (b) C. K. Chiang, A. J. Heeger, and A. G. MacDiarmid, *Ber. Bunsenges. Phys. Chem.*, **83**, 407 (1979), and references therein.

(30) (a) W. Shockley, "Electrons and Holes in Semiconductors", Van Nostrand, Princeton, 1950; (b) F. Beleznay, G. Biczó, and J. Ladik, *Acta Phys. Hung.*, **18**, 213 (1963); (c) M. Kertész, J. Koller, and A. Azman, *Chem. Phys.*, **27**, 273 (1978).

(31) See, e.g., G. Güner, *Chem. Scr.* **17**, 207 (1981).

(32) F. H. Herbstein, M. Kaftory, M. Kapon, and W. Saenger, *Z. Kristallogr.*, **154**, 11 (1981).

Chemical Reaction Paths. 8.[1] Stereoisomerization Path for Triphenylphosphine Oxide and Related Molecules: Indirect Observation of the Structure of the Transition State

Erik Bye,[2] W. Bernd Schweizer, and Jack D. Dunitz*

Contribution from the Organic Chemistry Laboratory, Swiss Federal Institute of Technology, ETH-Zentrum, CH-8092 Zürich, Switzerland. *Received February 2, 1982*

Abstract: The conformations of more than 1000 Ph_3PX molecules or molecular fragments have been retrieved from the Cambridge Crystallographic Data Centre Database. Each observed conformation is regarded as a sample point defined by the rotation angles of the three phenyl groups. From the distribution of such sample points conclusions may be drawn about features of the molecular potential energy surface. In particular, we have been able to chart out low-energy stereoisomerization paths for triphenylphosphine oxide (and related molecules) and to discern the approximate structure of the transition state for this stereoisomerization process.

In this paper we apply the structure correlation method[3,4] to map low-energy stereoisomerization paths for molecules of the type Ph_3PX, e.g., triphenylphosphine oxide and related molecules or fragments of molecules, including metal complexes of triphenylphosphine. Such isomerizations involve mainly rotations of the phenyl groups, and hence we shall be interested mainly in the torsion angles around the three Ph–P bonds. Indeed, we shall

(1) Part 7. Britton, D.; Dunitz, J. D. *J. Am. Chem. Soc.* **1981**, *103*, 2971–2979.

(2) On leave of absence from University of Oslo in 1977. Address correspondence to Institute of Occupational Health, Box 8149, Oslo 1, Norway.

(3) (a) Bürgi, H. B. *Inorg. Chem.* **1973**, *12*, 2321–2325. (b) Murray-Rust, P.; Bürgi, H. B.; Dunitz, J. D. *J. Am. Chem. Soc.* **1975**, *97*, 921–922.

(4) Dunitz, J. D. "X-Ray Analysis and the Structure of Organic Molecules"; Cornell University Press: Ithaca, NY, 1979; Chapter 7.

0002-7863/82/1504-5893$01.25/0

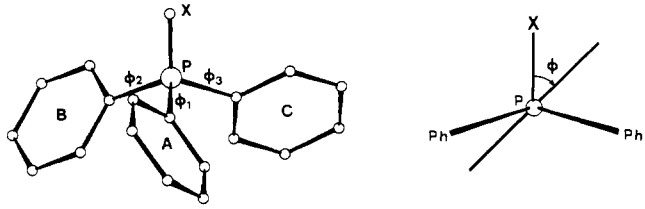

Figure 1. Left: The arbitrary conformation of a Ph_3P–X fragment is specified by three torsion angles $\omega_A = \varphi_1$, $\omega_B = \varphi_2$, $\omega_C = \varphi_3$ where the phenyl groups are labeled A, B, C, in a clockwise sequences when viewed down the X–P direction. Right: Definition of torsion angle φ.

Table I. General and Special Positions (Modulo 2π) for Isometric Conformations of a Molecule Composed of Three Phenyl Groups on a C_{3v} Frame[a]

no. of positions	point symmetry[b]	coordinates of equivalent positions (modulo 2π) $(0, 0, 0; \pi, 0, 0; 0, \pi, 0; 0, 0, \pi;$ $0, \pi, \pi; \pi, 0, \pi; \pi, \pi, 0; \pi, \pi, \pi)+$
48	1	$\varphi_1, \varphi_2, \varphi_3; \varphi_3, \varphi_1, \varphi_2; \varphi_2, \varphi_3, \varphi_1;$ $-\varphi_1, -\varphi_3, -\varphi_2; -\varphi_3, -\varphi_2, -\varphi_1; -\varphi_2, -\varphi_1, -\varphi_3$
24	2	$\pi/2, \varphi, -\varphi; -\varphi, \pi/2, \varphi, \varphi, -\varphi, \pi/2$
24	2	$0, \varphi, -\varphi; -\varphi, 0, \varphi; \varphi, -\varphi, 0$
16	3	$\varphi, \varphi, \varphi; -\varphi, -\varphi, -\varphi$
8	32	$\pi/2, \pi/2, \pi/2$
8	32	0, 0, 0

[a] The space group of the conventional unit cell is $R32$. [b] The point symmetries refer to the conformational map, not to the corresponding molecular conformations.

regard each observed Ph_3PX fragment as a sample point $\mathbf{p}(\varphi_1,\varphi_2,\varphi_3)$, where φ_1, φ_2, and φ_3 are values of these torsion angles, and we shall assume that sample points tend to concentrate in low-energy regions of the corresponding three-dimensional space. This is, in fact, the central assumption of the structure correlation method.

The present work includes two new features. One concerns the symmetry properties of the sample-point distributions. Since torsion angles are cyclic coordinates, these distributions have periodic character and their symmetry properties are then most conveniently described in terms of space groups. The underlying concepts have been sketched by Murray-Rust, Bürgi, and Dunitz[5] and discussed in more detailed by Dunitz.[6] The second new aspect is the attempt to describe the structure of a transition state from the sample-point distributions, i.e., from experimental data.

Definitions and Concepts

An arbitrary conformation of a Ph_3P–X fragment is specified by three torsion angles, $\omega_A = \varphi_1$, $\omega_B = \varphi_2$, $\omega_C = \varphi_3$, where the labels A, B, C, each refer to a given phenyl group, the sequence of labels being taken as clockwise when viewed down the X–P direction, as in Figure 1. Zero torsion angle is taken when the phenyl group in question eclipses the C–P bond, and increasing φ corresponds to clockwise rotation of the phenyl group, viewed along the bond from the central P atom. An idealized Ph_3P–X molecule would have C_{3v} point symmetry if all three torsion angles were zero or 90°. Even for arbitrary conformations, it is still useful to think of the three phenyl groups as rigid rotors on a C_{3v} frame. The symmetry operations of the frame then convert a given conformation into a set of equivalent, isometric conformations, or, what is the same, they convert a representative point $\mathbf{p}(\varphi_1,\varphi_2,\varphi_3)$ into a set of equivalent points:

	E	C_3	C_3^2	σ_A	σ_B	σ_C
ω_A	φ_1	φ_3	φ_2	$-\varphi_1$	$-\varphi_3$	$-\varphi_2$
ω_B	φ_2	φ_1	φ_3	$-\varphi_3$	$-\varphi_2$	$-\varphi_1$
ω_C	φ_3	φ_2	φ_1	$-\varphi_2$	$-\varphi_1$	$-\varphi_3$

(5) Murray-Rust, P.; Bürgi, H. B.; Dunitz, J. D. *Acta Crystallogr., Sect. A* **1979**, *35*, 703–713.
(6) Chapter 10 of ref 4.

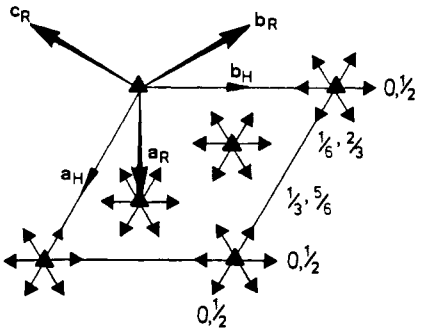

Figure 2. Primitive rhombohedral cell (space group $R32$) in hexagonal coordinate system: $\mathbf{a}_H = \mathbf{a}_R - \mathbf{b}_R$, $\mathbf{b}_H = \mathbf{b}_R - \mathbf{c}_R$, $\mathbf{c}_H = \mathbf{a}_R + \mathbf{b}_R + \mathbf{c}_R$. The hexagonal cell has lattice points at 0, 0, 0; $^2/_3, ^1/_3, ^1/_3$; $^1/_3, ^2/_3, ^2/_3$. The threefold axes are indicated by triangles. The twofold axes, whose directions are indicated by broad arrows, occur in pairs separated by $\mathbf{c}_H/2$; the numbers give the fractional z_H coordinates.

Table II. General and Special Positions (Modulo π) Referred to Hexagonal Coordinates (cf. Table I)[a]

no. of positions	point symmetry	coordinates of equivalent positions (modulo π) $(0, 0, 0; 2\pi/3, \pi/3, \pi/3; \pi/3, 2\pi/3, 2\pi/3)+$
18	1	$x, y, z; -y, x-y, z; y-x, -x, z; y, x, -z;$ $-x, y-x, -z; x-y, -y, -z$
9	2	$x, 0, \pi/2; 0, x, \pi/2; -x, -x, \pi/2$
9	2	$x, 0, 0; 0, x, 0; -x, -x, 0$
6	3	$0, 0, z; 0, 0, -z$
3	32	$0, 0, \pi/2$
3	32	0, 0, 0

[a] Hexagonal coordinates are (in terms of torsion angles): $x_H = (2\varphi_1 - \varphi_2 - \varphi_3)/3$; $y_H = (\varphi_1 + \varphi_2 - 2\varphi_3)/3$; $z_H = (\varphi_1 + \varphi_2 + \varphi_3)/3$.

These points can be immediately identified with the set of general equivalent positions (modulo 2π) of the three-dimensional space group $R32$. In addition to the frame-symmetry operations, flips of the phenyl groups through 180° also lead to isometric conformations; the list of equivalent positions (modulo 2π) then has to be extended to take account of these operations, which correspond to translations of the representative point. A complete list of general and special positions is given in Table I. Note that a noncyclic permutation of the torsion angles, e.g., $\varphi_1, \varphi_2, \varphi_3 \rightarrow \varphi_1, \varphi_3, \varphi_2$, does not correspond to a symmetry operation of the frame group, and neither does reversal of the signs of the three torsion angles $\varphi_1, \varphi_2, \varphi_3 \rightarrow -\varphi_1, -\varphi_2, -\varphi_3$. That is to say, molecules described by $\varphi_1, \varphi_2, \varphi_3$ and by $\varphi_1, \varphi_3, \varphi_2$ (or $-\varphi_1, -\varphi_2, -\varphi_3$) are not, in general, isometric. For visualization purposes it is more convenient to use hexagonal rather than rhombohedral axes (Figure 2). The transformation from rhombohedral ($\mathbf{q}_R$) to hexagonal ($\mathbf{q}_H$) basis vectors is $\mathbf{q}_H = \mathbf{M}\cdot\mathbf{q}_R$ with

$$\mathbf{M} = \begin{vmatrix} 1 & -1 & 0 \\ 0 & 1 & -1 \\ 1 & 1 & 1 \end{vmatrix}$$

and the corresponding hexagonal coordinates are

$$x_H = (2\varphi_1 - \varphi_2 - \varphi_3)/3 \qquad y_H = (\varphi_1 + \varphi_2 - 2\sigma_3)/3$$
$$z_H = (\varphi_1 + \varphi_2 + \varphi_3)/3 \tag{1}$$

with the inverse transformation

$$\varphi_1 = x_H + z_H$$
$$\varphi_2 = -x_H + y_H + z_H$$
$$\varphi_3 = -y_H + z_H$$

Note that a molecule with torsion angles $\varphi, \varphi, \varphi$ corresponds to a point with hexagonal coordinates 0, 0, φ.

General and special positions referred to the nonprimitive hexagonal cell are given in Table II. See Dunitz[6] for more detailed discussion of these points.

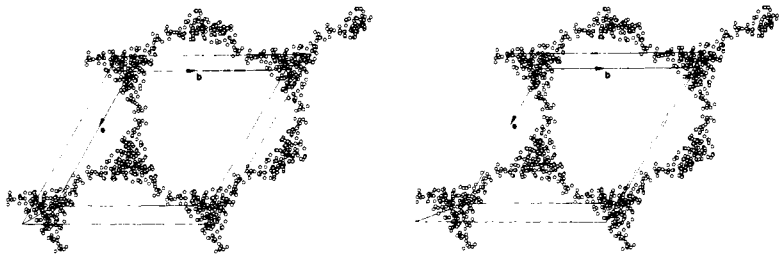

Figure 3. Stereoscopic view of distribution of Ph_3PO sample points in a section of the hexagonal cell with $0 \le z_H \le 60°$ (drawn by computer program PLUTO78[7]). The unit translations of the hexagonal cell are 180°.

Data Retrieval and Reduction

The experimental information for our analysis was taken from the Cambridge Crystallographic Database,[7] version of September 1981, with 30058 entries in the bibliographic file.[8]

A search in the connectivity file for Ph_3P fragments (unsubstituted phenyl groups) gave a total of 982 hits, leading to 1021 entries in the data file. Of these 441 were eliminated because atomic coordinates were unavailable or unreliable (error flag!) or because the crystal structure was regarded as not sufficiently precise for our purpose (disorder, or reliability index R greater than 0.15). This left 580 entries dealing with 560 compounds and containing 1114 Ph_3PX fragments.[9]. Since the Ph_3PX stereoisomerization path can be expected to vary somewhat depending on the nature of X, it seemed prudent to subdivide the data accordingly and treat each subgroup as a separate distribution. In order to give reasonably well-defined distributions in three-dimensional space, the number of fragments in each subgroup should not be too small. For X = N, O, Mn, Fe, Ni, Cu, Ru, Rh, Pd, Ag, Os, Ir, Pt, and Au, we obtained more than 20 structural fragments in each class, and the subsequent discussion is limited to those data.

In our model the three phenyl groups are regarded as rotors on a C_{3v} frame. The actual frames (consisting of the X atom, the P atom, and the three directly bonded α-C atoms) often show quite considerable deviations from this ideal symmetry, particularly in the P–X direction (the differences in the C–P–X angles range up to 20°). It was therefore necessary to symmetrize each frame by replacing the actual P–X vector by one pointing along the approximate threefold axis relating the P–C bonds. For each fragment the following sequence of calculations were made (steps 1–3 with program GEOM 78).[7]

1. The three α-C atoms were provisionally labeled C_A, C_B, C_C subject to the condition that the torsion angle P–C_A–C_B–C_C was positive. This ensured that the sequence of labels was clockwise when viewed down the X–P direction, or, in other words, that P–C_A, P–C_B, and P–C_C formed a right-hand-coordinate system.
2. A dummy atom D was placed at the centroid of C_A, C_B, and C_C.
3. For every phenyl group, the two torsion angles t_i(D–P–C–C_i), i = 1, 2, involving the α-C atom and the two ortho-C atoms were calculated. For a perfectly planar phenyl group these should differ by π. The ring torsion angle was then taken as the positive quantity $\varphi = (t_1 + t_2 + \pi)/2$. This angle is the same as if t_1 and t_2 had been calculated as $t(D'$–P–C–$C_i)$ with P–D′ in the opposite direction to P–D, i.e., in the same direction as P–X.
4. The phenyl group associated with the largest value of $\varphi = \varphi_1$ was taken as ring A. The clockwise sequence then defines rings B and C.
5. Hexagonal coordinates x_H, y_H, z_H were calculated from φ_1, φ_2, φ_3. A particular point (x_H, y_H, z_H) will not in general lie in the asymmetric unit with $0 \le x_H, y_H, z_H \le 60°$ but can always be transformed into a symmetry-related point that has this property (see Table II). Note that after this transformation, a further transformation back to φ_1, φ_2, φ_3 will not necessarily give positive values for the three torsion angles.
6. The quantity $d = (x_H^2 + y_H^2 - x_H y_H)^{1/2}$ was calculated. This is the distance of the point from the triad axis passing through the origin and hence a measure of the deviation of the fragment from C_3 symmetry, i.e., from an ideal propeller.

Results

Table III gives torsion angles, hexagonal coordinates, P–O distances, average P–C distances, average C–P–O angles, and deviations from C_3 symmetry (expressed in degrees) for the triphenylphosphine oxide fragments listed under their Cambridge Crystallographic Database acronyms. The corresponding information for the other Ph_3P–X fragments is contained in supplementary Tables S1–S13,[10] and is summarized in Table IV.

Table IV shows that when X is a metal atom, P–X distances lie in the range 2.2–2.4 Å and are much longer than P–O or P–N distances, which have mean values of 1.50 and 1.58 Å, respectively. Even for a given X, the scatter of P–X distances about the mean value is larger for the metals than for O or N, the rms deviations being typically 0.04–0.06 Å for the metals, 0.02 Å for O, and 0.03 Å for N. While we have made no attempt to judge the quality of the individual crystal structure analyses, the standard deviations of the individual values estimated from least-squares criteria invariably show the opposite trend, i.e., smaller for the P–metal distances than for P–O and P–N. Besides, these estimated standard deviations are much smaller than the rms deviations from the means. This suggests that the large scatter in M–X distances originates more from an intrinsic spread than from inaccuracies in the analyses, and, indeed, with the exception of the oxides, the chemical environments of the Ph_3P–X fragments do vary enormously from one structure to another. For example, fragments with X = N include imines, phosphazenes, iminium salts, etc., and we have not tried to distinguish among these in our classification, similarly for the fragments where X is a metal atom.

However, in spite of this heterogeneity within classes, and in spite of the variation in P–X distances, the P–C distances and C–P–X angles do not differ much, either within a given class or even between classes. The classes with X a metal atom show mean P–C distances of 1.82–1.84 Å with rms deviations of 0.01–0.02 Å within classes; for X = O or N, the P–C distances are slightly shorter, 1.79 Å for O, 1.80 Å for N, with rms deviations of about 0.01 Å. There is a similar trend in the C–P–X angles, which have mean values of 114 to 116° when X is a metal atom and 111° when X is O or N. The decrease in C–P–X angle corresponds to an increase in the C–P–C angle and just about compensates for the decrease in the P–C length in keeping the distance between the α-C atoms roughly constant.

We now examine the distribution of sample points $\mathbf{p}(x_H,y_H,z_H)$, remembering that each point is the image of a Ph_3PX molecule with torsion angles φ_1, φ_2, φ_3 related to x_H, y_H, z_H by eq 1. For Ph_3PO fragments the distribution corresponding to the data in

(7) Cambridge Crystallographic Data Centre, University Chemical Laboratories, Cambridge, England. For a recent bibliography see footnote 9 of ref 1.

(8) A preliminary study was made earlier using the version of Sept 1976 with 15157 entries in the bibliographic file. This led to conclusions similar to those reported here but not as convincing; see p 474 of ref 4.

(9) For entries containing more than one Ph_3PX fragment, any additional fragments containing substituted phenyl groups are not automatically eliminated by program GEOM 78.[7] They had to be removed by inspection of the individual entries, and it is possible that a few may have eluded our scrutiny. Our conclusions would not be seriously altered thereby.

(10) See paragraph at end of paper regarding supplementary material.

Table III. Relevant Structural Parameters for 62 Ph_3PO Fragments Listed under Their Cambridge Crystallographic Database Acronyms

TABLE FOR PH3-P-O

NO	REFCODE	TORSION ANGLES PHI1	PHI2	PHI3	HEXAGONAL COORD. X	Y	Z	BOND DISTANCES P-O	⟨P-C⟩	BOND ANGL ⟨C-P-O⟩	DISTANCE FROM C3
1	ACPOXU	41.	28.	18.	12.	11.	29.	1.48	1.79	111.	11.
2	AIXPOU	51.	35.	39.	9.	2.	42.	1.47	1.79	110.	8.
3	AIXPOU	85.	30.	-8.	50.	44.	35.	1.48	1.81	111.	47.
4	BTZANI	38.	38.	38.	0.	0.	38.	1.44	1.79	114.	0.
5	CACPOU	32.	38.	15.	4.	13.	29.	1.53	1.81	111.	12.
6	CDXUPO	53.	41.	39.	8.	5.	45.	1.52	1.79	111.	7.
7	CLPHOU	39.	51.	20.	2.	17.	36.	1.49	1.79	111.	16.
8	CLPHOU	64.	25.	28.	25.	11.	39.	1.50	1.79	111.	22.
9	CLTPOC	72.	24.	17.	34.	20.	38.	1.50	1.80	111.	30.
10	CLTPOC	72.	24.	18.	34.	20.	38.	1.50	1.80	111.	29.
11	CTPOCU	76.	24.	12.	39.	25.	37.	1.49	1.80	111.	34.
12	CXPHOU	44.	49.	38.	0.	6.	44.	1.50	1.79	111.	6.
13	CXPHOU	87.	22.	0.	51.	36.	36.	1.50	1.79	112.	45.
14	DBTPOC	84.	24.	-2.	48.	37.	35.	1.53	1.81	111.	44.
15	DBTPOC	91.	14.	2.	55.	34.	35.	1.50	1.82	112.	48.
16	ECOPPU20	48.	30.	33.	11.	4.	37.	1.49	1.82	114.	10.
17	ETPLAP10	60.	26.	35.	20.	5.	40.	1.49	1.83	113.	18.
18	ETPSMP10	59.	8.	24.	29.	6.	30.	1.51	1.82	114.	26.
19	ETPSMP10	71.	50.	23.	22.	25.	48.	1.50	1.82	113.	24.
20	LABTSA10	56.	33.	34.	15.	7.	41.	1.51	1.78	111.	13.
21	MALTPO	56.	21.	20.	24.	12.	32.	1.49	1.79	112.	20.
22	MALTPO	69.	32.	30.	25.	14.	43.	1.49	1.81	112.	22.
23	MSIALA	52.	35.	38.	10.	4.	42.	1.51	1.77	111.	9.
24	NTPOCE	60.	35.	8.	26.	26.	34.	1.53	1.81	110.	26.
25	NTPOCE	43.	38.	29.	6.	8.	37.	1.53	1.82	110.	7.
26	NTPOTH	57.	38.	12.	21.	24.	36.	1.43	1.80	108.	23.
27	NTPOTH	45.	36.	31.	8.	6.	37.	1.47	1.80	112.	7.
28	PPOHAU	66.	39.	41.	18.	8.	49.	1.53	1.78	110.	15.
29	TCPOXU	45.	52.	16.	7.	22.	38.	1.48	1.74	114.	19.
30	TCPOXU	51.	9.	15.	26.	10.	25.	1.49	1.75	113.	23.
31	TCPOXU	72.	20.	32.	31.	10.	42.	1.47	1.75	111.	27.
32	TCPOXU	56.	35.	32.	15.	9.	41.	1.48	1.78	112.	13.
33	TCPOXU	45.	31.	14.	15.	16.	30.	1.52	1.80	112.	15.
34	TCPOXU	83.	14.	-8.	54.	38.	30.	1.46	1.79	113.	48.
35	TCPOXU	66.	9.	-5.	43.	28.	23.	1.51	1.77	110.	38.
36	TCPOXU	49.	37.	40.	7.	3.	42.	1.52	1.77	113.	6.
37	TFPOND	71.	11.	15.	39.	18.	32.	1.50	1.80	111.	33.
38	TFPOND	43.	51.	17.	6.	20.	37.	1.49	1.81	112.	18.
39	TPEPHO	59.	21.	25.	24.	10.	35.	1.46	1.76	112.	21.
40	TPEPHO01	78.	20.	11.	41.	25.	36.	1.49	1.83	113.	36.
41	TPEPHO02	77.	19.	11.	41.	24.	36.	1.48	1.79	112.	36.
42	TPOBII10	84.	20.	-11.	54.	42.	31.	1.51	1.80	112.	49.
43	TPOBII10	36.	25.	20.	9.	7.	27.	1.50	1.81	111.	8.
44	TPOCLU10	53.	40.	40.	9.	4.	44.	1.52	1.80	110.	7.
45	TPOPHX	41.	19.	27.	12.	2.	29.	1.53	1.78	110.	11.
46	TPOPHX	63.	36.	28.	21.	14.	43.	1.52	1.78	111.	18.
47	TPOPHX01	43.	17.	29.	13.	1.	30.	1.53	1.79	110.	13.
48	TPOPHX01	66.	36.	30.	22.	14.	44.	1.52	1.79	111.	19.
49	TPOTCA	54.	47.	13.	16.	25.	38.	1.50	1.80	112.	22.
50	TPOXHF	56.	21.	29.	21.	6.	35.	1.50	1.79	111.	18.
51	TPPOBR	56.	11.	21.	27.	8.	29.	1.48	1.79	111.	24.
52	TPPOBR	24.	24.	21.	1.	2.	23.	1.50	1.79	111.	2.
53	TPPOCU	69.	10.	11.	39.	19.	30.	1.49	1.80	110.	34.
54	TPPOCU	34.	30.	14.	9.	12.	26.	1.47	1.80	112.	11.
55	TPPOHG	65.	29.	12.	30.	23.	35.	1.50	1.79	111.	27.
56	TPPOHG	56.	49.	30.	11.	15.	45.	1.53	1.77	111.	14.
57	TPPOHG	42.	12.	2.	23.	16.	19.	1.51	1.81	109.	21.
58	TPPOPH	77.	33.	12.	36.	29.	41.	1.48	1.79	112.	33.
59	TPPOSE	66.	17.	33.	27.	5.	39.	1.52	1.80	112.	25.
60	TPPOSE	58.	30.	33.	18.	8.	41.	1.50	1.80	112.	16.
61	TPPOSN	58.	42.	27.	16.	16.	42.	1.47	1.81	112.	16.
62	TPPOUC10	82.	25.	5.	45.	32.	37.	1.53	1.77	108.	40.
	MEAN							1.50	1.79	111.	

Table III is shown in the stereoviews, Figures 3 and 4. Figure 3 is a slice through the hexagonal cell with $0 \leq z_H \leq 60°$, viewed down the c_H axis; Figure 4 is a view of the clusters around the threefold axes at 0, 0, z_H; 120°, 60°, z_H; 180°, 0°, z_H with $0 \leq z_H \leq 60°$.

Figure 3 shows a vast empty rregion around the special position 60°, 120°, 30°, which is the image of a molecule with torsion angles 90°, 90°, −90°, i.e., all three phenyl rings perpendicular to the respective C–P–O planes, evidently a region of high potential energy. The equivalent special position 0, 0, 90° (halfway along c axis, see Figure 4) is the image of a molecule with torsion angles 90°, 90°, 90°. As seen in Figure 4, there is another empty region surrounding 0, 0, 0, the image of a molecule with all three rings lying exactly in the C–P–O planes. On the other hand, the points

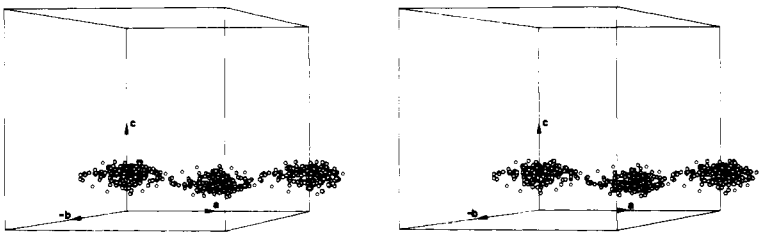

Figure 4. As in Figure 3, but showing clusters of sample points centered at 0, 0, 40°; 120°, 60°, 20°; 180°, 0°, 40°, viewed along a direction approximately perpendicular to $\mathbf{a}_H$.

Table IV. Mean P–X Distance, P–C Distance, and C–P–X Angles in Ph_3P–X Fragments with a Common X Atom[a]

	d(P–X), Å	d(P–C), Å	∠C–P–X, deg	n
N	1.58 (3)	1.80 (1)	111 (2)	85
O	1.50 (2)	1.79 (1)	111 (2)	62
Mn	2.32 (5)	1.83 (1)	115 (2)	21
Fe	2.25 (4)	1.83 (1)	115 (2)	30
Ni	2.22 (7)	1.84 (2)	115 (2)	47
Cu	2.25 (5)	1.83 (1)	115 (2)	58
Ru	2.36 (5)	1.84 (2)	116 (2)	75
Rh	2.31 (6)	1.83 (1)	115 (3)	78
Pd	2.32 (5)	1.83 (1)	115 (2)	38
Ag	2.43 (6)	1.82 (2)	114 (2)	29
Os	2.38 (4)	1.83 (1)	114 (2)	22
Ir	2.34 (4)	1.83 (1)	115 (2)	86
Pt	2.29 (4)	1.83 (2)	115 (3)	148
Au	2.30 (5)	1.82 (2)	114 (2)	42

[a] n is the number of fragments in each class after removal of symmetry-equivalent fragments. Quantities in brackets are root-mean-square deviations from the means. Individual fragments are listed in Table III (X = O) and in Supplementary Tables S1–S13.

cluster densely around the threefold axes 0, 0, $z_H \sim 40°$ and symmetry-equivalent regions (images of molecules with approximately C_3 symmetry), and the paths that interconnect these dense regions are also clearly recognizable in both Figures 3 and 4.

Figure 5 is a histogram, constructed from the data of Table III, showing the relative frequencies of Ph_3PO sample-points in successive 10° intervals of d (measure of deviation from C_3 symmetry) along a projected radius emanating from the threefold axis 0, 0, z_H.[11] This histogram strongly suggests that the equilibrium conformation of an isolated Ph_3PO molecule has C_3 symmetry or very close to it.[12]

The interconnecting paths are then the paths for the stereoisomerization of a given molecule with C_3 symmetry into its enantiomer. In the range $0 \le z_H \le 60°$ sample points close to the triad axis 0, 0, z_H are images of molecules in which all three rings are rotated clockwise (those with positive torsion angles, as listed in Table III), while those close to the triad axis 120°, 60°, z_H are images of the corresponding enantiomers. For example, the point **p** = 0, 0, 40° is the image of a molecule with torsion angles 40°, 40°, 40°, and the point **p** = 120°, 60°, 20° is the image of the enantiomeric molecule with torsion angles 140°, −40°, −40°. The point **p** = 60°, 30°, 30°, exactly midway between these, is the image of the molecule with torsion angles 90°, 0°, 0°, an achiral conformation with C_s symmetry.

The stereoisomerization path evidently starts out in the general direction of this midpoint but then tends to avoid it, taking a course with a somewhat larger y_H coordinate. Moreover, there is clearly a gradual thinning out of sample-points in this intermediate region of the path. According to our basic assumption, the density of sample points along the path should decrease as the energy rises. This enables us to identify the transition state for the stereoisomerization reaction as lying in the least densely populated stretch of the reaction path close to **p** = 60°, 40°, 30°, the image of a molecule with torsion angles approximately 90°, 10°, −10°. In the initial stage of the stereoisomerization of our representative molecule with torsion angles 40°, 40°, 40°, one torsion angle, say ω_A, increases while the other two decrease by about half the amount. As ω_A approaches 90° the retrorotation of the other two rings is no longer synchronous, ring B rotating less than ring C to reach the transition state around (ω_A, ω_B, ω_C =) 90°, 10°, −10°, corresponding to a mirror-symmetric structure. Whether the transition state is actually mirror-symmetric (image of a point on the dyad axis of the space group) or only approximately so is impossible to decide from this kind of information. At any rate, the mirror-symmetric structure must correspond to a turning point in the energy, so it must either be an energy minimum between a pair of equivalent transition states or an energy maximum, but in the latter event it may lie not quite on the reaction path.

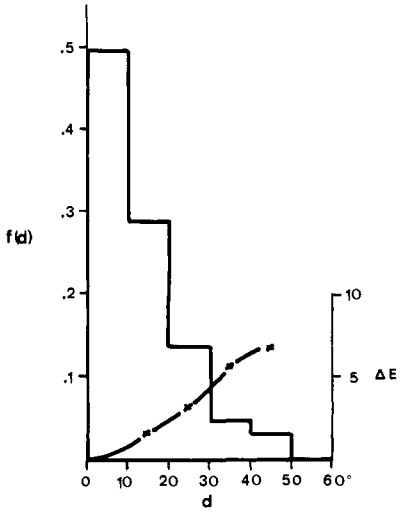

Figure 5. Histogram constructed from the data of Table III showing relative frequency $f(d)$ of Ph_3PO sample points in successive 10° intervals of d along a central line, assuming circular symmetry. Also shown (–x–) are the corresponding energy increments ΔE estimated from Boltzmann distribution with RT arbitrarily taken as 2.42 kJ mol^{-1}.

It is tempting to interpret the distribution of sample points around the equilibrium C_3 conformation as resulting from a Boltzmann-like distribution. This appealing though scarcely justifiable assumption would give a kind of quasi-quantitative expression to our belief that sample points tend to accumulate in low-energy regions and avoid high-energy regions of the corresponding space. However, we do not know what effective temperature to use in the expression $\exp(-\Delta E/RT)$. Figure 5 shows the energy increments ΔE that are obtained by arbitrarily setting RT = 2.42 kJ mol^{-1} (corresponding to T around room temperature). With these assumptions the energy of molecules in the 50–60° range, where the transition state lies, would be about 6–8 kJ mol^{-1}. As far as we are aware, no experimental value of the activation energy for the stereoisomerization of Ph_3PO is available for comparison to calibrate the energy scale empirically.

Very similar distributions of sample points are obtained for the other classes. In all cases there are empty regions similar to those seen in Figures 3 and 4 for the oxides and in roughly the same

(11) The implicit assumption of circular symmetry in the distribution of sample points is, of course, only correct for infinitesimally small d and becomes increasingly worse as d increases.

(12) For some of the other classes, particularly those with X = Rh, Pd, Pt, the corresponding distributions suggest that the equilibrium conformations may not have C_3 symmetry. However, they still have approximate C_3 symmetry in the sense that all three phenyl groups are rotated in the same direction.

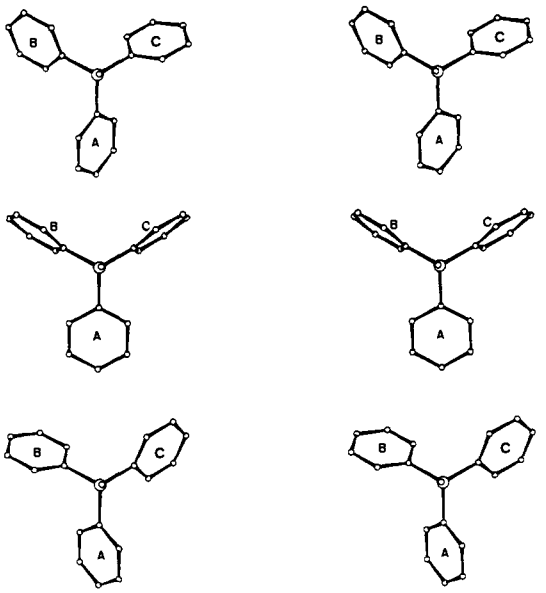

Figure 6. Stereoscopic views of three structures along the stereoisomerization path: (top) C_3 symmetric equilibrium structure with torsion angles 40°, 40°, 40°; (center) mirror-symmetric transition state with torsion angles 90°, 10°, −10°; (bottom) C_3 symmetric equilibrium structure with torsion angles −40°, −40°, −40°, the enantiomer of the top structure.

parts of the unit cell. In all cases, the densely populated regions are found in parts of the unit cell that are also populated fairly heavily in the oxides. In all cases, the reaction path for the stereoisomerization is at least qualitatively similar to that found for the oxides with an avoidance of the midpoint **p** = 60°, 30°, 30° and a similar thinning-out of sample points in the intermediate region to indicate the presence of a transition state close to **p** = 60°, 40°, 30°. Insofar as it is possible to estimate the activation energies from these kinds of data, they are also roughly similar to that found for the oxides or even a little lower in some cases. In some classes, e.g., X = Pt, Ni, Ru, Rh, there are a few experimental points that occur in regions of the sample space which are normally empty. The corresponding molecular structures contain several Ph_3P fragments and are so sterically hindered that it would be virtually impossible to achieve low-energy conformations for all the fragments.

Recapitulation and Discussion

In this work we have mapped the reaction path for the stereoisomerization of triphenylphosphine oxide and its congeners from experimental data derived from many hundreds of crystal-structure analyses. The equilibrium structure of an isolated Ph_3P–X fragment is close to a symmetric propeller shape with all three phenyl rings rotated from the respective C–P–X planes in the same sense and by approximately the same amount, about 40°. Starting with a molecule with positive torsion angles (Figure 6), the stereoisomerization path begins by a rotation of one ring, say A, toward 90° (perpendicular to its C–P–X plane) coupled with a rotation of the other two rings in the opposite sense (toward 0°) and by about half the amount of ring A. As the reaction proceeds, the rotation of the other two rings B and C gets out of step, ring B (clockwise from A, Figure 6) rotating less than ring C to reach a mirror-symmetric structure with torsion angles approximately 90°, 10°, −10°. At this point, ring A has rotated by +50°, ring B by −30°, ring C by −50°. In the second part of the path, the roles of ring B and ring C are interchanged, so the path ends at the enantiomorphic structure with torsion angles 140°, −40°, −40° equivalent to −40°, −40°, −40°.

This itinerary is based on experimental distributions of sample points for which Figures 3 and 4 (for Ph_3PO fragments) are typical. There is a noticeable thinning-out of sample points in the intermediate regions around **p** = 60°, 40°, 30° corresponding to the mirror-symmetric structure with torsion angles 90°, 10°, −10°, and we therefore identify this structure or one very close to it as the transition state for the stereoisomerization in question. Although putative structures for transition states have been often obtained from *calculations* at various levels of sophistication and complexity for many types of chemical reactions, we believe that this is the first time the structure of a transition state has been determined in such detail from *experimental* data. Of course, our method is very indirect and it is probably limited to only a few types of reaction for which sufficiently extensive crystal-structure data are available and which are unlikely to be of outstanding chemical interest. But still.

In principle, the reaction path for the stereoisomerization of triphenylphosphine derivatives could also be derived by suitable force-field calculations, but these do not seem to have been carried out so far. Andose and Mislow[13] have described results of such calculations for the stereoisomerization of trimesitylmethane, a somewhat cognate molecule that also has as its equilibrium conformation a propeller with torsion angles about 40°. In these calculations one ring was driven from its equilibrium orientation by a succession of incremental rotations and the other structural parameters were allowed to relax so as to minimize the energy. The isomerization path of lowest energy corresponded to what was called the "two-ring flip" mechanism; in our nomenclature this involves the passage of one ring through torsion angle 90° and of the other two rings through 0°—in agreement with our findings for the Ph_3PX fragments.[14] Depending on which ring was driven in the calculations, two slightly different paths were obtained, each with its own transition state: one with torsion angles 75°, 10°, −22° (A), the other with torsion angles 92°, 35°, −38° (B) in our nomenclature. In hexagonal coordinates these occur at $\mathbf{p}_A$ = 54°, 43°, 21° (with a symmetry related point at $\mathbf{p}_A$, = 66°, 17°, 39°) and $\mathbf{p}_B$ = 62°, 68°, 30°. Andose and Mislow concluded that the actual transition state lies somewhere near these calculated points, a property shared by our transition state at **p** = 60°, 40°, 30°. While there is no reason to believe that the stereoisomerization paths for trimesitylmethane and for triphenylphosphine oxide should coincide, one can expect them to be at least of the same general type and to differ only in detail. Thus the qualitative agreement between the calculated transition state for one reaction and the experimentally derived one for the other is reassuring.

Acknowledgment. We are grateful to Professor H.B. Bürgi for pertinent criticism. We also thank the Swiss Government and the Norwegian Research Council for Science and the Humanities (NAVF) for the award of fellowships to E.B. during the year 1977.

Registry No. Ph_3PO, 791-28-6.

Supplementary Material Available: Tables S1–S13 listing torsion angles, φ_1, φ_2, φ_3; hexagonal coordinates, x_H, y_H, z_H; P–X and ⟨P–C⟩ distances, ⟨C–P–X⟩ angles, $d = (x_H^2 + y_H^2 - x_H y_H)^{1/2}$ for X = N, Mn, Fe, Ni, Cu, Ru, Rh, Pd, Ag, Os, Ir, Pt, Au (21 pages). Ordering information is given on any current masthead page.

(13) Andose, J. D.; Mislow, K. *J. Am. Chem. Soc.* **1974**, *96*, 2168–2176.
(14) The two-ring flip mechanism is also indicated by dynamic NMR studies of variously substituted triarylboranes, triarylmethanes, and cognate molecules in solution. See K. Mislow, *Acc. Chem. Res.* **1976**, *9*, 26–33, for a review of the experimental evidence and its interpretation.